
CSI-Net: Unified Human Body Characterization and Pose Recognition

Fei Wang*

Xi'an Jiaotong University
Carnegie Mellon University
feiwang@cmu.edu

Jinsong Han

Xi'an Jiaotong University
Zhejiang University
hanjinsong@zju.edu.cn

Shiyuan Zhang

Xi'an Jiaotong University
shiyangzhang932@gmail.com

Xu He

Xi'an Jiaotong University
hexu.xjtu@gmail.com

Dong Huang

Carnegie Mellon University
donghuang@cmu.edu

Abstract

We build CSI-Net, a unified Deep Neural Network (DNN), to learn representation of WiFi signals. Using CSI-Net, we jointly solved two body characterization problems: biometrics estimation (including body fat, muscle, water and bone rates) and person recognition. We also demonstrated the application of CSI-Net on two distinctive pose recognition tasks: the hand sign recognition (fine-scaled action of the hand) and falling detection (coarse-scaled motion of the body). Code has been made publicly at <https://github.com/geekfeiw/CSI-Net>.

1 Introduction

Recent years witness rapid growth of techniques using Channel State Information (CSI) of WiFi signals in sensing human bodies. These techniques lead to major boost of applications in human-computer interaction [1, 2, 3], health care[4, 5, 6, 7] and surveillance[8, 9, 10]. Comparing to computer vision based human sensing, WiFi-based techniques enable non-line-of-sight activity recognition[10], allow prevalent deployment in daily living and working environment, and arises little privacy concern.

The core problem of WiFi sensing is to prepare a proper representation of signals that directly correlates with human body characteristics and activities. Existing work used hand-crafted features: (1) Temporally aligned CSI sequences by Dynamic Time Wrapping (DTW)[11, 12, 13, 14, 3, 15]. (2) Statistical features of the CSI sequences, such as the average, variance, and entropy. It is unclear how to manually design person-specific features for body characteristics and person-invariant features for activities. Moreover, the interaction of WiFi signals with human body and background results in complex multi-path transmission, reflection and attenuation of CSI, making it extremely difficult for hand-craft feature to extract delicate information from CSI data.

On the other hand, recent advances of deep learning exhibit extraordinary ability in learning data representation from data. There are some preliminary attempts on indoor localization[16] and person recognition[17]. However, to our knowledge, no existing work has build a unified deep learning framework that solves multiple WiFi sensing problems.

The technical contribution of this paper can be summarized as follows.

1. We propose CSI-Net, a deep learning framework for human sensing with WiFi CSI sequences.

*Work done when at Robotics Institute, CMU.

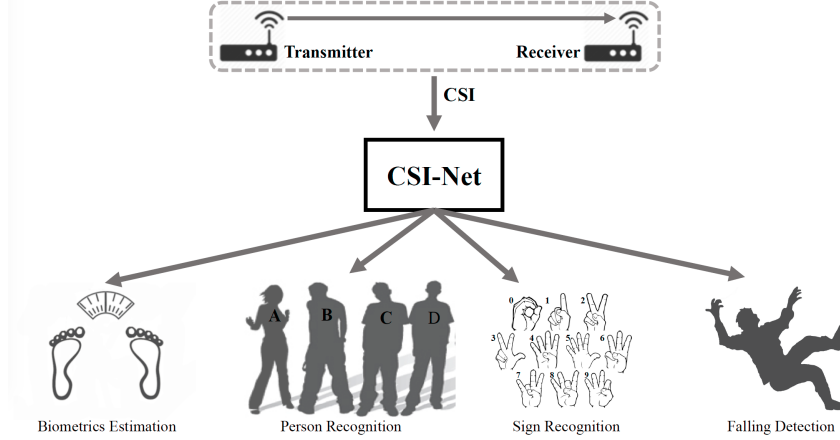


Figure 1: System overview. CSI is generated from the transmitter/receiver WiFi communication. CSI-Net is a unified body characterization and activity recognition deep learning architecture. In this paper, we apply CSI-Net to do body characterization tasks such as biometrics estimation and person recognition, meanwhile, we also apply it to do activity recognition tasks such as hand sign recognition and falling detection.

2. We solve a variety of human sensing tasks using CSI-Net: biometrics estimation, person recognition, hand sign recognition and falling detection.
3. We qualitatively analyze the influence of person body on WiFi signals and build a database for CSI-based human sensing tasks.

2 Related Work

2.1 Body Characterization

The majority of CSI-based body characterization work focuses on person recognition [18, 19, 20, 21, 22, 23]. These work use walking pattern to identify person identity. Specifically, subjects are asked to walk along a predefined path repeatedly while the CSI sequences are recorded as training data. Then classification algorithms are developed to map the CSI data to identities. In these approaches, computing discriminative representation for each user is very difficult yet essential to the identification performance. In [19, 20, 21, 22, 23], statistical features, e.g., *maximum*, *minimum*, *mean*, *energy* and *entropy*, are extracted from the CSI sequences and fed to classifiers, e.g., Support Vector Machine(SVM), for person recognition. In these work, feature representations of CSI are manually designed, and it is difficult to guarantee that features are discriminative for person recognition.

2.2 Activity Recognition

In terms of processing flow, recent approaches in CSI-based activity recognition fall into two main schemas. **(1) Feature classification:** *raw CSI* -> *filtered CSI* -> *hand-crafted features* (statistical features)-> *classifier* -> *activity classes* [24, 5]. **(2) Sequence matching:** *raw CSI* -> *filtered CSI* -> *dynamic time wrapping (DTW)* [25] -> *k-nearest neighbors (kNN)* -> *activity prediction*. The former schema has shortages in designing task-specifically features. The later schema requires computing distances between a testing CSI and every training CSI, which is very time-consuming. In addition, kNN algorithm is generally inferior to a supervised learning classifier.

2.3 Bio-electromagnetics in WiFi Signal Band

Our work is based on fundamental principles in Bio-electromagnetics. Bio-electromagnetics studies the changes of electromagnetic (EM) waves when encountering biological bodies. Many literatures specifically studied the Bio-electromagnetics in WiFi Signal Band, e.g., 2.4G WiFi (2470MHz-2544MHz) and 5G WiFi (5033MHz-6006MHz). In [26], dielectric parameters like permittivity

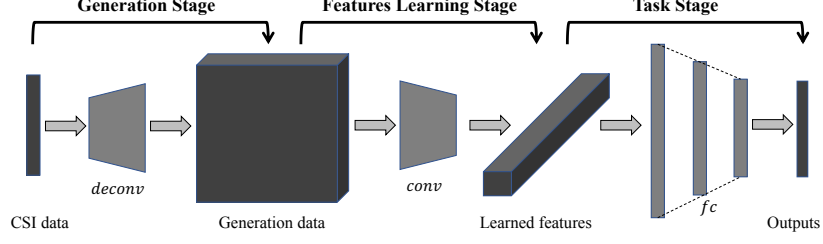


Figure 2: Architecture of CSI-Net.

and conductivity of body tissues, such as fat, muscle and liver *etc.*, were measured within the EM frequency of 10Hz to 20GHz. In [27, 28, 29], human body is modeled as layered tissues with different dielectric parameters. [30] also used the layered tissue model to compute the power decay and time delay of EM wave when propagating through human body at the frequency of 2.45GHz. This work provides critical cues to measure human body spatially, making it possible to capture body gestures/actions using the decayed and delayed WiFi signals.

3 Network Architecture

As shown in Fig. 2, CSI-Net is composed of three functional components: the generation stage, the feature learning stage and the task stage. The generation stage transforms CSI data to feature maps with the spatially-encoded patterns. The feature learning stage further maps the spatially-encoded patterns to the features for sensing tasks. Finally, the features are used to produce outputs in the task stage.

3.1 Input Tensor of CSI-Net

CSI is computed from a channel estimation process in the 802.11 n/g WiFi system. Using [31], we can extract CSI as a complex-valued sequence, $\mathbf{A} \in \mathcal{C}^{N_{sa} \times N_{sc} \times N_{tx} \times N_{rx}}$, where N_{sa} and N_{sc} are the number of sampled WiFi packets and number of subcarriers, respectively. N_{tx} and N_{rx} are number of transmitting and receiving antennas, respectively. In our setting, $N_{sc} = 30$, $N_{tx} = 1$ and $N_{rx} = 1$.

We take the CSI at each sampling time-stamp as a multi-channel tensor, $(a_i \in \mathcal{C}^{30 \times 1 \times 1}, i \in [1, N_{sa}])$. Due to the unstable CSI phases, we only use CSI amplitudes.

3.2 Generation Stage

Using transposed convolution (TC), also called deconvolution, we build a generation stage of CSI-Net. The generation stage explore the within-channel for spatial information CSI-Net input tensors while make it possible to take advantages of modern DNN architectures on images. TC is widely used in Generative Adversarial Nets (GANs) to for image generation [32, 33]. Specifically, We here stack 8 transposed convolution layers to process the $30 \times 1 \times 1$ input tensor, and produce a tensor of $6 \times 224 \times 224$. The target tensor size is set to 224×224 is because it is a common input size of CNN architectures excluding VGG-nets [34], Inception[35] and ResNets[36], hence easier in tuning hyperparameters.

3.3 Features Learning Stage

Feature learning stage takes the $6 \times 224 \times 224$ tensor from the generation stage and extracts features for final tasks. Following the fashion in computer vision, we call the networks in feature learning stage as the backbone network. Given image-like tensors after the generation stage, various modern CNN architectures, such as AlexNet [37], VGG-nets[34], Inception clusters[35, 38, 39, 40], ResNets[36], and DenseNet [41] can be potentially used as backbone with slight revisions. Following insights in [42], we select ResNet for it is generally more powerful than AlexNet, has less parameters than VGG-nets, Inception Net and DenseNet.

3.4 Task Stage

The task stage is to leverage features learned above to compute the outputs for a specific task. It is composed of several fully-connected layers, activation function and loss function.

Fully-connected layers re-weight the features to produce an output vector for a task. As shown in Table 1, to estimate 4 biometrics, *i.e.*, human body fat rate, muscle rate, water rate and bone rate, the output dimension is 4. Person recognition is conducted among 30 subjects, so the output dimension is 30. In our experiments, we only use one fully-connected layer.

In the biometrics estimation task, we use Rectified Linear Unit (ReLU)[43] plus L1 to compute loss. In other tasks, the SoftMax activation and Cross Entropy function are combined to generate loss.

Data Sizes / Tasks	Biometrics Estimation	Person Recognition	Sign Recognition	Falling Detection
CSI-Net Input	$30 \times 1 \times 1$	$30 \times 1 \times 1$	$30 \times 1 \times 1$	$30 \times 1 \times 1$
Generation Stage	$6 \times 224 \times 224$	$6 \times 224 \times 224$	$6 \times 224 \times 224$	$6 \times 224 \times 224$
Feature Learning Stage	256	256	128	128
Task Stage	4	30	10	2
CSI-Net Output	4	30	10	2

Table 1: Tensor sizes at different stages of CSI-Net.

3.5 Configuration on Different Tasks

For different sensing tasks, the output functions and intermediate tensors are different, as illustrated in Table 1. Taking the task of biometrics estimation as an example, the input tensor size is $Channel \times Height \times Width : 30 \times 1 \times 1$. After the generation stage, the tensor is $6 \times 224 \times 224$. Then, 256 features are extracted by the feature learning stage. At last, the task stage estimate four biometrics (4 scalars) from the 256 features. The output tensor size of CSI-Net is equal to the output size of task stage. More implementation details of CSI-Net on different sensing tasks are presented in Section 4.

4 Implementation Details

In this section, we present the implementation details of CSI-Net, including the preparing dataset and training CSI-Net.

System Settings/ Tasks	Biometrics Estimation	Person Recognition	Sign Recognition	Falling Detection
Tx-Rx Height	1.2m	1.2m	0.8m	0.8m
Tx-Rx Distance	1.6m	1.6m	0.6m	3.0m
# of Subjects	30	30	1	1
Subject Body Pose	standing	standing	sitting	standing&laying
# of Positions	1	1	1	5
Sampling Duration	100s	100s	60s	30s
Sampling Rate	100Hz	100Hz	100Hz	100Hz
CSI Samples	300K	300K	60K	30K
Center Frequency	5GHz	5GHz	5GHz	5GHz

Table 2: System settings in experiments.

4.1 Preparing Datasets

The dataset preparation consists of testbed setup, CSI collection, filter design, training/test data split and data augmentation.

4.1.1 Testbed setup

We employed Commodity Off-The-Shelf (COTS) devices to setup our testbed. We replaced the network interface card (NIC) with Intel 5300 NIC at 2 mini-PCs. Both of them were installed with Linux 802.11n CSI Tool [31] for parsing CSI. More setup details are listed in Table 2.

4.1.2 CSI data collection

CSI samples were recorded when subjects keep stationary poses or gestures during data collection. The CSI sampling rate was set to 100Hz for all tasks below.

Biometrics Estimation: we recruited 30 subjects, measured some biometrics of their bodies with Mi® body composition scale[44], and listed the information in the Table 10. We selectively estimated the body fat rate and body muscle rate because these two metrics indicates what the body shape a person has. We also estimated the water rate and bone rate, which are essentially related to the human body internal composition.

Person Recognition: we reused the sampled CSI for biometrics estimation to identify human. Actually, we trained a CSI-Net with 2 separate task stages, one for biometrics estimation and another for person recognition, with the same inputs.

Sign Recognition: for a proper comparison with non-adapted DNNs work, we imitated the experiment setting shown in a prior work [2] to collect CSI dataset for hand sign recognition. The imitations include the same selection of hand signs, height of Tx and Rx, and distance between Tx and Rx, even similarly asking subjects to sit on a chair *etc.*

Falling Detection: we selected 5 positions in the room and asked one subject to act action of standing and laying (the duration of each action is about 30 seconds), where the laying was to simulate the human body state of fallen down.

4.1.3 Training/Testing sets.

In all tasks, we used the first 4/5 CSI sequences for training and the remaining 1/5 for testing. We took this splitting strategy to simulate the practical scenarios, where one first collects data and trains a network, then tests incoming data.

We propose a data augmentation method, shown in Algorithm 1. The main idea is to deliberately introduce some jitter CSI to the training data, so that CSI-Net can learn to model more data variances. Thus, it would be more resilient to the unpredictable CSI in the test phase.

Algorithm 1: Data Augmentation

Input: Original Training Set: $S = \{s_1, s_2, \dots, s_n\}$
Output: Augmented Training Set: S'
Initialize $S' = \{\}$
for $k \in [2, 3, 5, 7]$ **do**
 Shuffle $S \rightarrow S^* = \{s_1^*, s_2^*, \dots, s_n^*\}$
 Initialize $S_k = \{\}$
 for $i \in [1, 2, \dots, \lfloor n/k \rfloor]$ **do**
 Average k continuous shuffled instances $\frac{1}{k} \sum_{(i-1)k+1}^{ik} s_i^* \rightarrow s'_i$
 $s'_i \cup S_k \rightarrow S_k$
 end
 $S_k \cup S' \rightarrow S'$
end
 $S' \cup S \rightarrow S'$

Sets /Tasks	Biometrics Estimation	Person Recognition	Sign Recognition	Falling Detection
#Training instances	38,633	38,633	21,428	21,879
#Test instances	4,444	4,444	2,468	2,519

Table 3: The training/test “Sets” for four sensing tasks. For example, the tasks of biometrics estimation and person recognition used 38,633 training instances and 4,444 test instances, respectively.

4.2 Loss Function

Biometrics Estimation and Person Recognition: We set the *loss* of the jointly-trained tasks, denoted with L , as follows,

$$L = L_{bio} + \alpha L_{id} \quad (1)$$

where L_{bio} and L_{id} are the *losses* of biometrics estimation and person recognition, respectively. α works as a importance balance between both tasks. L_{bio} is the sum of 4 biometrics estimation *losses* that are computed by L1 Loss, and the L_{id} is computed by the Cross Entropy Loss. Following settings in Fast R-CNN[45], we normalize the biometrics values within [0,1] before training, meanwhile, we set the balance α to 1.

Sign Recognition: We compute the *loss* of hand sign recognition by

$$L = -\log p_i \quad (2)$$

where p_i is the i -th SoftMax result of an instance that is with a true label of i . Actually, this is one of writing styles of the Cross Entropy Loss.

Falling Detection: The Cross Entropy Loss is also applied to compute the *loss* of falling detection task.

4.3 Training Networks

CSI-Net was implemented in *Pytorch* 0.4.1 and trained on a Ubuntu server with 4 Titan Xp GPUs. The optimizer is Adam[46] with default parameters ($\beta_1 = 0.9, \beta_2 = 0.999$). We train the networks for 20 epochs with a minibatch size of 20 and initial learning rate of 0.001. The learning rate is decayed by 10% at the epoch of {4, 7, 10, 13, 16, 18}.

5 Evaluation

In this section, we first present accuracies of CSI-Net on 3 classification tasks, *i.e.*, person recognition, sign recognition and falling detection, and make a comparison with prior work. Then we depict CSI-Net performance on all 4 tasks detailedly. Besides, We show some discoveries about behaviors of CSI-Net processing CSI data. We also list the performance of 9 different backbone networks, including ResNet-152, Inception-V4 and VGG-19. We find that ResNet-18 performed best for our datasets. In addition, we modify the generation stage and propose a new version of CSI-Net.

5.1 Accuracy Comparison

We show accuracies of CSI-Net on 3 classification tasks, *i.e.*, person recognition, hand sign recognition and falling detection, in Table 4. Meanwhile, accuracies achieved by Support Vector Machine (SVM) and Naïve Bayes, are listed as the baseline. For SVM, we use LibSVM[47] with radial basis function kernel ($\gamma = 1/30$), L2 regularization and penalty of 1. Naïve Bayes is implemented with assumption that CSI data follows Gaussian distribution. Features used in SVM and Naïve Bayes are the CSI amplitudes of 30 subcarriers, similar to the CSI-Net. The only difference is that the input size of CSI-Net is $30 \times 1 \times 1$, but the input size of SVM and Naïve Bayes is 30×1 .

Method	Accuracy		
	Person Recognition	Sign Recognition	Falling Detection
CSI-Net	93.00%	100%	96.67%
SVM-RBF	85.28%	90.24%	81.46%
Naïve Bayes	72.97%	81.00%	73.01%
Prior work	79.28%-50[18], 80%-6[19], 91%-11[17]	90.2%[2], 93%[14]	90%[24], 91.5% [5], 93%[11]

Table 4: Classification accuracy comparison. Existing work on person recognition were conducted on different number of subjects, denoted as $xx\% - \#subjects$.

We see accuracies of CSI-Net on three classification tasks are 93.00%, 100% and 96.67%, respectively. Apparently, CSI-Net outperforms SVM and Naïve Bayes in all three tasks. Comparison with closely-related prior work is also shown in Table 4, illustrating that CSI-Net is an alternative method to do different tasks. Besides, CSI-Net is able to jointly estimate human biometrics with identification.

5.2 Biometrics Estimation

To evaluate the results of biometrics estimation, we apply two metrics, *i.e.*, mean average error (*mAE*) and mean square deviation (*mSD*). The former is to measure the estimation error of CSI-Net, and the latter for the estimation variance. The *mAE* is computed as follows.

$$e_k = \frac{1}{N_k} \sum_{i=1}^{N_k} |s_{k,i}^* - s_{k,i}| \quad (3)$$

where the e_k represents the average estimation error of the k -th subject, $s_{k,i}$ stands for the real i -th test value of the k -th subject, $s_{k,i}^*$ represents the estimation value, and N_k is the volume of test data of the k -th subject. The metric, *mAE*, is the *mean* of all average estimation errors ($e_k, k \in [1, 30]$).

$$mAE = \frac{1}{30} \sum_{k=1}^{30} e_k \quad (4)$$

mSD is computed in a similar way.

	Fat Rate	Muscle Rate	Water Rate	Bone Rate
<i>mAE</i>	1.11	1.00	0.71	0.38
<i>mSD</i>	0.58	0.50	0.24	0.07
min-max range	[5.0, 30.9]	[65.2, 89.9]	[49.2, 65.1]	[1.6, 13]

Table 5: The mean Average Error (*mAE*) and mean Square Deviation(*mSD*) of four biometrics estimation tasks.

As shown in Table 5, CSI-Net achieves very small *mAEs* and *mSDs* comparing to the numerical range of 30 subjects' biometrics. Taking the fat rate estimation result as an example, the average estimation error is 1.11, which can be considered as a small error because the min-max range of fat rate is [5.0, 30.9], as listed in Table 10. Besides, the estimating variance is 0.58, indicating that CSI-Net has an excellent performance in terms of stability. The results demonstrate that human body does incur strong CSI variance which can be effectively utilized to estimate the human biometrics.

In Fig. 3, we draw a set of radar charts to visualize the estimated biometrics of 30 subjects. In each chart, the four axes (right/up/left/down) correspond to four human biometrics (fat/muscle/water/bone rate). In the figure, the red lines stand for the average estimation values. The green lines represent the ground truth of biometrics measured by the Mi® body composition scale[44]. The majority of blue lines are perfectly overlapped with the red lines, implying that CSI-Net can estimate biometrics accurately for every subject.

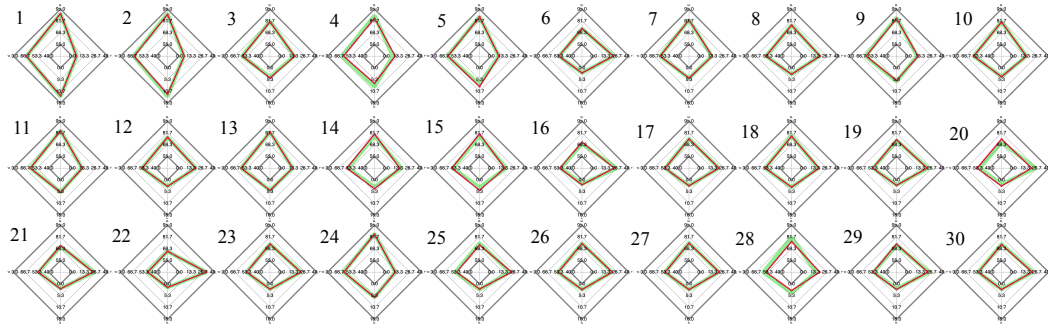


Figure 3: Radar charts of biometrics estimation for 30 subjects. Four axes (right/up/left/down) correspond to four human biometrics (fat/muscle/water/bone rate), the red lines are estimation, the green lines are ground-truth.

5.3 Person Recognition

We evaluate person recognition results with the confusion matrix in Fig. 4. The column label is the real human ID and the row label is the predicted human ID. The gray level of block (i, j) represents

the ratio that the j -th subject is identified as the i -th subject by CSI-Net. From the figure, we observe that CSI-Net achieves 100% accuracy on most of subjects.

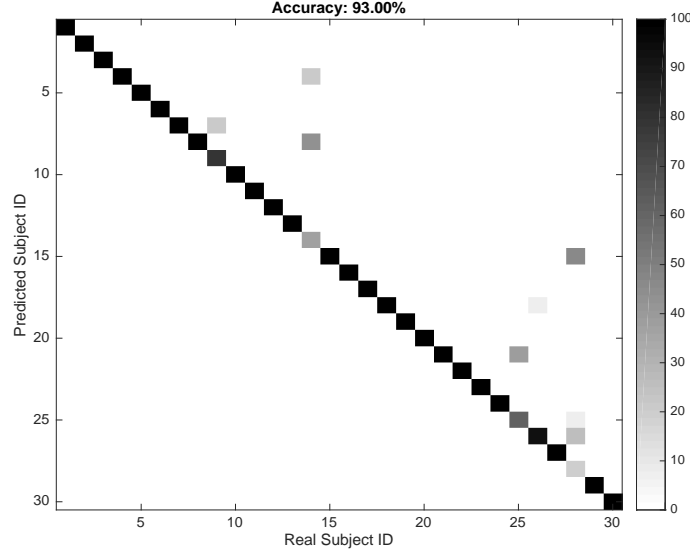


Figure 4: Confusion matrix of person recognition for 30 subjects.

5.4 Sign Recognition

We also illustrated the results of hand sign recognition with a confusion matrix in Fig. 5. The column label is the real hand sign and the row label is the predicted hand sign. In this figure, we find that using our dataset CSI-Net achieves an accuracy of 100%. This extremely high accuracy demonstrates that micro human postures can result in CSI variances. Meanwhile, even the variances caused by very similar hand sign gestures can be well recognized by CSI-Net.

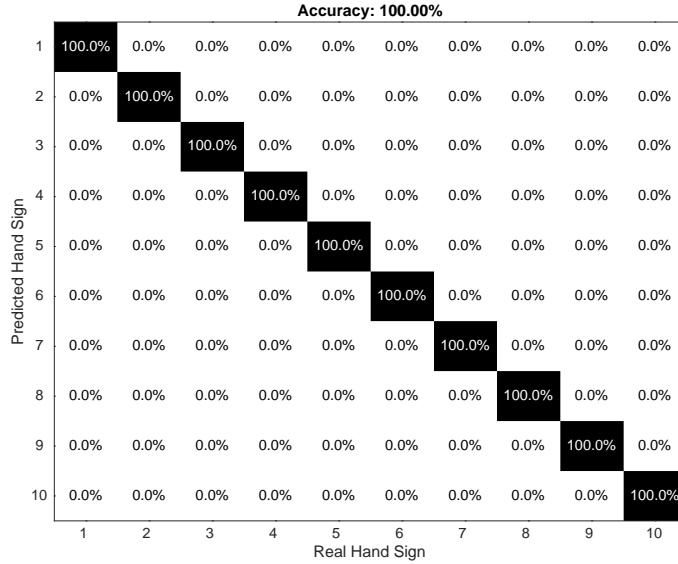


Figure 5: Confusion matrix of sign recognition. CSI-Net predicted sign of $\{0, 2, 3, 4, 5, 6, 7, 8, 9\}$ with 100% accuracy. Only 5.6% error occur where some “1”s were recognized as “8”.

5.5 Falling Detection

The results of falling detection task are listed in Table 6, where the accuracy of CSI-Net detecting falling is 98.73%. In practice, this is a high detection accuracy. Still, CSI-Net wrongly predicts falling activities to standing case with ratio of 1.27%, and incorrectly thinks standing case as falling activities with ratio of 5.41%. This incorrect detection can be solved with a little longer monitoring duration, which allows the system has more samples to vote for a detection results. Here, we do not tend to go deeper in this system optimization, because it is out of main scope of this paper.

	Real Falling	Real Standing
Detected Falling	1246 (98.73%)	68 (5.41%)
Detected Standing	16 (1.27%)	1189 (94.59%)

Table 6: Confusion matrix of falling detection. CSI-Net predicted falling and standing with accuracy of 98.73% and 94.59%, respectively. The error occurs where it predicts 1.27% of falling to standing, and predicts 5.41% of standing to falling.

5.6 Ablation Experiments

All above results are obtained with the backbone of ResNet-18 [36]. As explained in Section 3, CSI-Net is a scalable architecture and can be easily combined with other good CNN networks, such as VGG-net [34] and Inception [40]. Next, we report the results achieved by these backbones and show that ResNet-18 produced the best results for our datasets, shown in Table 7. In addition, ResNet-18 is the smallest model, shown in Table 8. We believe that ResNet-18 gives the best balance between model complexity and data complexity.

backbone	Person Recognition		Sign Recognition		Falling Detection	
	acc (train)	acc (test)	acc (train)	acc (test)	acc (train)	acc (test)
ResNet-18	100%	93.00%	100%	100%	98.13%	96.67%
ResNet-34	100%	85.10%	98.74%	72.69%	96.02%	94.40%
<i>ResNet-50</i>	99.99%	87.51%	99.99%	100%	95.77%	93.85%
<i>ResNet-101</i>	100%	88.41%	99.96%	99.03%	96.14%	93.33%
ResNet-152	100%	88.61%	100%	100%	94.07%	89.68%
<i>Inception-V3</i>	99.94%	82.63%	100%	100%	97.04%	96.35%
<i>Inception-V4</i>	100%	87.60%	100%	100%	96.11%	93.01%
VGG-16	30.03%	18.70%	80.31%	46.67%	87.63%	83.56%
VGG-19	19.03%	16.00%	75.27%	42.30%	88.83	85.15%

Table 7: Result of different backbones. “acc(train)” and “acc(test)” represent training accuracy and test accuracy, respectively.

backbone	Person Recognition	Sign Recognition	Falling Detection
ResNet-18	88MB	61MB	61MB
<i>ResNet-34</i>	127MB	102MB	102MB
ResNet-50	189MB	176MB	176MB
ResNet-101	798MB	366MB	366MB
ResNet-152	878MB	423MB	423MB
<i>Inception-V3</i>	90MB	90MB	90MB
<i>Inception-V4</i>	164MB	164MB	164MB
VGG-16	975MB	531MB	531MB
VGG-19	995MB	552MB	552MB

Table 8: Saved model size.

5.7 Deconvolution or Interpolation

In the generation stage of CSI-Net, 8 stacked transposed convolution layers convert the CSI data to a tensor with height/width 224×224 , which is approximating to conventional input size of CNNs. However, considering the computation cost of these layers, we explored simpler but still efficient ways to reshape CSI into image-like tensors for CNNs. Then, we had a better deep architecture for our tasks. Next, we shown this update.

The first method is to resize CSI tensor from size of $30 \times 1 \times 1$ to size of $30 \times 224 \times 224$ with *bilinear* interpolation, whose performance is shown in Table 9. Surprisingly, this simple method achieves high accuracy in all tasks, which inspired us to reconsider the function of interpolation operation. We also replace the 2nd, 4th, 6th, and 8th layers with bilinear interpolations, resulting in a lighter CSI-Net. It outperforms the original CSI-Net with a notable increase in the accuracy. The results are shown in Table 9.

Method	Person Recognition		Sign Recognition		Falling Detection	
	acc (train)	acc (test)	acc (train)	acc (test)	acc (train)	acc (test)
Transposed Convolution (TC)	100%	93.00%	100%	100%	98.13%	96.67%
Interpolation (I)	100%	91.36%	100%	100%	98.12%	93.45%
CSI-Net V1.5 (TC+I)	100%	94.42%	100%	100%	98.07%	97.73%

Table 9: Three methods to make CSI sample image-like tensor. Interpolation means directly resizing $30 \times 1 \times 1$ CSI tensor to be $30 \times 224 \times 224$ with bilinear interpolation.

6 Conclusion

In this paper, we propose a wireless signal model to analysis CSI variance at the presence of human body. We conclude that human presence even without doing anything can introduce CSI variance, which can has significant potentials for sensing human problems. We elaborately design a unified CNN based networks, named CSI-Net, to handle the CSI data for a variety of sensing human takes. We deploy our approaches to test the conclusion and CSI-Net on body characterization and activity recognition, including four tasks: biometrics estimation, person recognition, hand sign recognition and falling detection. The experimental results show that all tasks can be achieved with distinguished performance. Deserved to be mentioned, our work is the first attempt to propose and achieve biometrics estimation using commodity WiFi devices, which has applicable potentiality on health care.

Acknowledge

We thank Wei Xi and Kun Zhao for discussion on WiFi properties. We thank Li Zhu, Pan Feng, Zhen Liao, Ziyi Dai and Yang Zi for their helps in data collection. Fei Wang is supported by China Scholarship Council.

References

- [1] K. Qian, C. Wu, Z. Zhou, Y. Zheng, Z. Yang, and Y. Liu, “Inferring motion direction using commodity wi-fi for interactive exergames,” in *Proceedings of the Conference on Human Factors in Computing Systems (CHI)*. ACM, 2017, pp. 1961–1972.
- [2] H. Li, W. Yang, J. Wang, Y. Xu, and L. Huang, “Wifinger: Talk to your smart devices with finger-grained gesture,” in *Proceedings of the International Joint Conference on Pervasive and Ubiquitous Computing (UbiComp)*. ACM, 2016, pp. 250–261.
- [3] K. Ali, A. X. Liu, W. Wang, and M. Shahzad, “Keystroke recognition using wifi signals,” in *Proceedings of the Annual International Conference on Mobile Computing and Networking (MobiCom)*. ACM, 2015, pp. 90–102.
- [4] B. Fang, N. D. Lane, M. Zhang, A. Boran, and F. Kawsar, “Bodyscan: Enabling radio-based sensing on wearable devices for contactless activity and vital sign monitoring,” in *Proceedings of the Annual International Conference on Mobile Systems, Applications and Services (MobiSys)*. ACM, 2016, pp. 97–110.

- [5] H. Wang, D. Zhang, Y. Wang, J. Ma, Y. Wang, and S. Li, "Rt-fall: a real-time and contactless fall detection system with commodity wifi devices," *Transactions on Mobile Computing (TMC)*, vol. 16, no. 2, pp. 511–526, 2017.
- [6] X. Wang, C. Yang, and S. Mao, "Tensorbeat: Tensor decomposition for monitoring multi-person breathing beats with commodity wifi," *arXiv preprint arXiv:1702.02046*, 2017.
- [7] H. Wang, D. Zhang, J. Ma, Y. Wang, Y. Wang, D. Wu, T. Gu, and B. Xie, "Human respiration detection with commodity wifi devices: Do user location and body orientation matter?" in *Proceedings of the International Joint Conference on Pervasive and Ubiquitous Computing (UbiComp)*. ACM, 2016, pp. 25–36.
- [8] W. Xi, J. Zhao, X.-Y. Li, K. Zhao, S. Tang, X. Liu, and Z. Jiang, "Electronic frog eye: Counting crowd using wifi," in *Proceedings of the International Conference on Computer Communications (INFOCOM)*. IEEE, 2014, pp. 361–369.
- [9] X. Zheng, J. Wang, L. Shangguan, Z. Zhou, and Y. Liu, "Smokey: Ubiquitous smoking detection with commercial wifi infrastructures," in *Proceedings of the International Conference on Computer Communications (INFOCOM)*. IEEE, 2016, pp. 1–9.
- [10] F. Adib and D. Katabi, "See through walls with wifi!" in *Proceedings of the SIGCOMM*. ACM, 2013, pp. 75–86.
- [11] S. Palipana, D. Rojas, P. Agrawal, and D. Pesch, "Falldefi: Ubiquitous fall detection using commodity wi-fi devices," *Proceedings of the Interactive, Mobile, Wearable and Ubiquitous Technologies (IMWUT)*, vol. 1, no. 4, p. 155, 2018.
- [12] H. Abdelnasser, M. Youssef, and K. A. Harras, "Wigest: A ubiquitous wifi-based gesture recognition system," in *Proceedings of the Conference on Computer Communications (INFOCOM)*. IEEE, 2015, pp. 1472–1480.
- [13] H. Abdelnasser, K. A. Harras, and M. Youssef, "Ubibreathe: A ubiquitous non-invasive wifi-based breathing estimator," in *Proceedings of the International Symposium on Mobile Ad Hoc Networking and Computing (MobiHoc)*. ACM, 2015, pp. 277–286.
- [14] S. Tan and J. Yang, "Wifinger: Leveraging commodity wifi for fine-grained finger gesture recognition," in *Proceedings of the International Symposium on Mobile Ad Hoc Networking and Computing (MobiHoc)*. ACM, 2016, pp. 201–210.
- [15] M. Li, Y. Meng, J. Liu, H. Zhu, X. Liang, Y. Liu, and N. Ruan, "When csi meets public wifi: Inferring your mobile phone password via wifi signals," in *Proceedings of the Conference on Computer and Communications Security (SIGSAC)*. ACM, 2016, pp. 1068–1079.
- [16] X. Wang, L. Gao, S. Mao, and S. Pandey, "Csi-based fingerprinting for indoor localization: A deep learning approach," *IEEE Transactions on Vehicular Technology*, vol. 66, no. 1, pp. 763–776, 2017.
- [17] C. Shi, J. Liu, H. Liu, and Y. Chen, "Smart user authentication through actuation of daily activities leveraging wifi-enabled iot," in *Proceedings of the International Symposium on Mobile Ad Hoc Networking and Computing (MobiHoc)*. ACM, 2017, p. 5.
- [18] W. Wang, A. X. Liu, and M. Shahzad, "Gait recognition using wifi signals," in *Proceedings of the International Joint Conference on Pervasive and Ubiquitous Computing (UbiComp)*. ACM, 2016, pp. 363–373.
- [19] Y. Zeng, P. H. Pathak, and P. Mohapatra, "Wiwho: Wifi-based person identification in smart spaces," in *Proceedings of the International Conference on Information Processing in Sensor Networks (IPSN)*. IEEE, 2016, p. 4.
- [20] J. Zhang, B. Wei, W. Hu, and S. S. Kanhere, "Wifi-id: Human identification using wifi signal," in *Proceedings of the International Conference on Distributed Computing in Sensor Systems (DCOSS)*. IEEE, 2016, pp. 75–82.
- [21] T. Xin, B. Guo, Z. Wang, M. Li, Z. Yu, and X. Zhou, "Freesense: Indoor human identification with wi-fi signals," in *Proceedings of the Global Communications Conference (GLOBECOM)*. IEEE, 2016, pp. 1–7.
- [22] J. Lv, W. Yang, D. Man, X. Du, M. Yu, and M. Guizani, "Wii: Device-free passive identity identification via wifi signals," in *Proceedings of the Global Communications Conference (GLOBECOM)*. IEEE, 2017, pp. 1–6.
- [23] Q. Xu, Y. Chen, B. Wang, and K. R. Liu, "Radio biometrics: Human recognition through a wall," *Transactions on Information Forensics and Security (TIFS)*, vol. 12, no. 5, pp. 1141–1155, 2017.
- [24] Y. Wang, K. Wu, and L. M. Ni, "Wifall: Device-free fall detection by wireless networks," *Transactions on Mobile Computing (TMC)*, vol. 16, no. 2, pp. 581–594, 2017.
- [25] D. J. Berndt and J. Clifford, "Using dynamic time warping to find patterns in time series," in *Proceedings of Data Mining and Knowledge Discovery (KDD), Workshop*, vol. 10, no. 16, 1994, pp. 359–370.

- [26] S. Gabriel, R. Lau, and C. Gabriel, "The dielectric properties of biological tissues: Ii. measurements in the frequency range 10 hz to 20 ghz," *Physics in Medicine and Biology*, vol. 41, no. 11, p. 2251, 1996.
- [27] A. Christ, T. Samaras, A. Klingenböck, and N. Kuster, "Characterization of the electromagnetic near-field absorption in layered biological tissue in the frequency range from 30 mhz to 6000 mhz," *Physics in Medicine & Biology*, vol. 51, no. 19, p. 4951, 2006.
- [28] A. Christ, A. Klingenböck, T. Samaras, C. Goiceanu, and N. Kuster, "The dependence of electromagnetic far-field absorption on body tissue composition in the frequency range from 300 mhz to 6 ghz," *IEEE transactions on microwave theory and techniques*, vol. 54, no. 5, pp. 2188–2195, 2006.
- [29] F. Wang, J. Han, Z. Dai, H. Ding, and D. Huang, "Wipin: Operation-free person identification using wifi signals," *arXiv preprint arXiv:1810.04106*, 2018.
- [30] I. Dove, "Analysis of radio propagation inside the human body for in-body localization purposes," Master's thesis, University of Twente, 2014.
- [31] D. Halperin, W. Hu, A. Sheth, and D. Wetherall, "Tool release: Gathering 802.11 n traces with channel state information," *SIGCOMM Computer Communication Review*, vol. 41, no. 1, pp. 53–53, 2011.
- [32] I. Goodfellow, J. Pouget-Abadie, M. Mirza, B. Xu, D. Warde-Farley, S. Ozair, A. Courville, and Y. Bengio, "Generative adversarial nets," in *Proceedings of the Advances in Neural Information Processing Systems (NIPS)*, 2014, pp. 2672–2680.
- [33] T. Salimans, I. Goodfellow, W. Zaremba, V. Cheung, A. Radford, and X. Chen, "Improved techniques for training gans," in *Proceedings of the Advances in Neural Information Processing Systems (NIPS)*, 2016, pp. 2234–2242.
- [34] K. Simonyan and A. Zisserman, "Very deep convolutional networks for large-scale image recognition," *arXiv preprint arXiv:1409.1556*, 2014.
- [35] C. Szegedy, W. Liu, Y. Jia, P. Sermanet, S. Reed, D. Anguelov, D. Erhan, V. Vanhoucke, A. Rabinovich *et al.*, "Going deeper with convolutions," in *Proceedings of the Conference on Computer Vision and Pattern Recognition (CVPR)*. IEEE, 2015.
- [36] K. He, X. Zhang, S. Ren, and J. Sun, "Deep residual learning for image recognition," in *Proceedings of the Conference on Computer Vision and Pattern Recognition (CVPR)*, 2016, pp. 770–778.
- [37] A. Krizhevsky, I. Sutskever, and G. E. Hinton, "Imagenet classification with deep convolutional neural networks," in *Proceedings of the Advances in Neural Information Processing Systems (NIPS)*, 2012, pp. 1097–1105.
- [38] S. Ioffe and C. Szegedy, "Batch normalization: Accelerating deep network training by reducing internal covariate shift," in *Proceedings of International Conference on Machine Learning (ICML)*, 2015, pp. 448–456.
- [39] C. Szegedy, V. Vanhoucke, S. Ioffe, J. Shlens, and Z. Wojna, "Rethinking the inception architecture for computer vision," in *Proceedings of the Conference on Computer Vision and Pattern Recognition (CVPR)*. IEEE, 2016, pp. 2818–2826.
- [40] C. Szegedy, S. Ioffe, V. Vanhoucke, and A. A. Alemi, "Inception-v4, inception-resnet and the impact of residual connections on learning," in *Proceedings of Association for the Advancement of Artificial Intelligence (AAAI)*, vol. 4, 2017, p. 12.
- [41] G. Huang, Z. Liu, K. Q. Weinberger, and L. van der Maaten, "Densely connected convolutional networks," in *Proceedings of the conference on Computer Vision and Pattern Recognition (CVPR)*, vol. 1, no. 2. IEEE, 2017, p. 3.
- [42] A. Canziani, A. Paszke, and E. Culurciello, "An analysis of deep neural network models for practical applications," *arXiv preprint arXiv:1605.07678*, 2016.
- [43] V. Nair and G. E. Hinton, "Rectified linear units improve restricted boltzmann machines," in *Proceedings of the International Conference on Machine Learning (ICML)*, 2010, pp. 807–814.
- [44] "Mi body composition scale," <http://www.mi.com/us/mi-body-composition-scale/>.
- [45] R. Girshick, "Fast r-cnn," *arXiv preprint arXiv:1504.08083*, 2015.
- [46] D. P. Kingma and J. Ba, "Adam: A method for stochastic optimization," *arXiv preprint arXiv:1412.6980*, 2014.
- [47] C.-C. Chang and C.-J. Lin, "LIBSVM: A library for support vector machines," *ACM Transactions on Intelligent Systems and Technology (TIST)*, vol. 2, pp. 27:1–27:27, 2011, software Available at <http://www.csie.ntu.edu.tw/~cjlin/libsvm>.
- [48] U. G. Kyle, I. Bosaeus, A. D. De Lorenzo, P. Deurenberg, M. Elia, J. M. Gómez, B. L. Heitmann, L. Kent-Smith, J.-C. Melchior, M. Pirlich *et al.*, "Bioelectrical impedance analysis—part i: Review of principles and methods," *Clinical Nutrition*, vol. 23, no. 5, pp. 1226–1243, 2004.

Appendix

Detailed CSI-Net Parameters

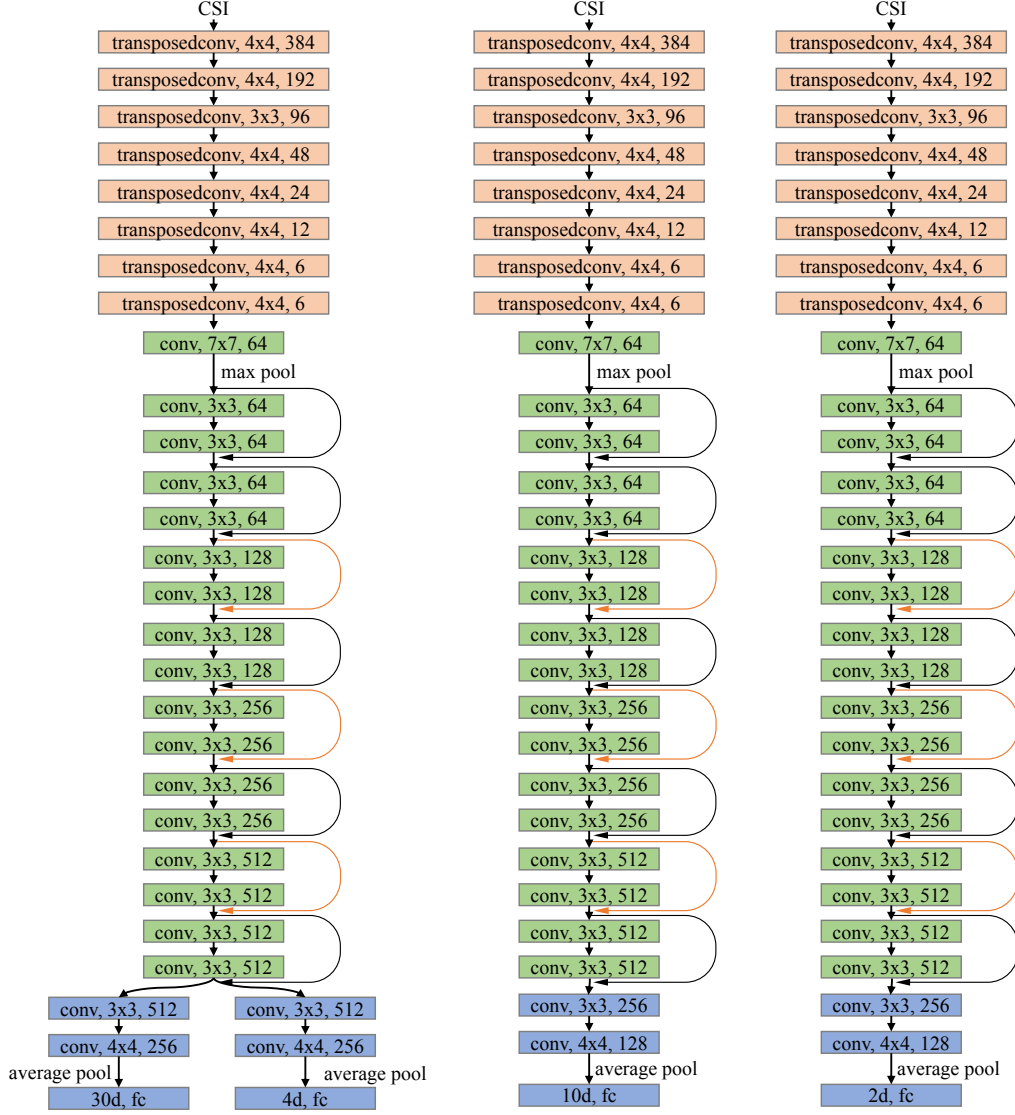


Figure 6: Sketches of CSI-Net architectures for tasks of, **Left:** joint biometrics estimation and person recognition. **Middle:** hand sign recognition, and **Right:** falling detection. The orange shortcuts increase channels. Please see <https://github.com/geekfeiw/CSI-Net> for a Pytorch implementation.

Subjects' Information

No.	Sex	Fat Rate (%)	Muscle Rate (%)	Water Rate (%)	Bone Rate (%)	Height (inches)	Weight (lbs)
1	Male	5.0	89.7	65.1	13.0	70.5	113.8
2	Male	5.0	89.9	65.1	13.0	66.1	107.9
3	Male	14.3	81.2	58.7	4.1	68.1	141.2
4	Male	7.3	87.8	63.5	8.7	68.5	121.0
5	Male	8.4	86.7	62.8	7.5	66.9	118.9
6	Female	22.9	72.8	52.8	2.3	62.6	104.7
7	Male	12.7	82.7	59.8	4.7	70.9	143.7
8	Male	18.9	76.9	55.6	2.9	71.3	161.7
9	Male	9.9	85.3	61.7	6.2	71.3	134.2
10	Male	15.0	80.5	58.2	3.9	65.0	127.9
11	Male	11.0	84.3	61.0	5.5	70.5	138.3
12	Male	18.9	76.8	55.6	2.9	66.9	148.2
13	Female	12.7	82.6	59.8	4.7	62.6	114.5
14	Female	17.5	78.0	56.5	3.2	63.8	105.4
15	Female	16.9	78.2	56.9	3.4	66.5	109.1
16	Female	26.2	69.4	50.6	1.9	63.4	121.9
17	Male	20.9	75.0	54.2	2.6	68.5	161.2
18	Female	17.2	78.3	56.7	3.3	64.2	105.9
19	Female	22.5	73.2	53.1	2.4	63.0	104.8
20	Male	25.1	70.9	51.3	2.0	71.7	190.5
21	Female	24.9	70.9	51.4	2.1	61.8	106.0
22	Female	30.9	65.2	49.2	1.6	60.6	118.4
23	Female	22.0	73.7	53.5	2.4	62.2	102.1
24	Male	10.1	85.2	61.6	6.1	69.3	128.9
25	Female	20.9	74.4	54.2	2.6	62.6	110.6
26	Female	20.8	74.4	54.2	2.6	65.4	110.6
27	Male	20.8	75.0	54.2	2.6	68.9	162.5
28	Male	14.4	81.1	58.6	4.1	66.9	135.4
29	Male	23.5	72.5	52.4	2.2	72.8	187.9
30	Male	22.3	73.6	53.2	2.4	65.0	152.7

Table 10: The information of 30 recruited subjects. All biometrics were measured using a body composition scale which embedded the module of Bioelectrical Impedance Analysis(BIA)[48]. Subjects were asked to stand on the scale after removing shoes and socks. All metrics were recorded when the reading of scale is stable.